Eur. Phys. J. A **6**, 471–477 (1999)

THE EUROPEAN PHYSICAL JOURNAL A

Recoil separator ERNA: ion beam specifications*

D. Rogalla[1], M. Aliotta[1,a], C.A. Barnes[2,b], L. Campajola[3], A. D'Onofrio[4], E. Fritz[1], L. Gialanella[1], U. Greife[1], G. Imbriani[3], A. Ordine[3], J. Ossmann[1], V. Roca[3], C. Rolfs[1], M. Romano[3], C. Sabbarese[4], D. Schürmann[1], F. Schümann[1], F. Strieder[1], S. Theis[1], F. Terrasi[4], H.P. Trautvetter[1]

[1] Institut für Physik mit Ionenstrahlen, Ruhr-Universität Bochum, Bochum, Germany
[2] California Institute of Technology, Pasadena, USA
[3] Dipartimento di Scienze Fisiche, Universita Federico II, Napoli and INFN, Napoli, Italy
[4] Dipartimento di Scienze Ambientali, Seconda Universita di Napoli, Caserta and INFN, Napoli, Italy

Received: 25 October 1999
Communicated by B. Povh

Abstract. For improved measurements of the key astrophysical reaction $^{12}C(\alpha,\gamma)^{16}O$ in inverted kinematics, a recoil separator ERNA is being developed at the 4 MV Dynamitron tandem accelerator in Bochum to detect directly the ^{16}O recoils with about 50% efficiency. Calculations of the ion beam optics including all filtering and focusing elements of ERNA are presented. Since the ^{12}C projectiles and the ^{16}O recoils have essentially the same momentum, and since the ^{12}C ion beam emerging from the accelerator passes through a momentum filter (analysing magnet), the ^{12}C ion beam must be as free as possible from ^{16}O contamination for ERNA to succeed. In the present work, the ^{16}O contamination was reduced from a level of 1×10^{-11} to a level below 2×10^{-29} by the installation of Wien filters both before and after the analysing magnet. The measurement of these and other beam specifications involved other parts of the final ERNA layout – sequentially a Wien filter, a 60° dipole magnet, another Wien filter, and a ΔE-E telescope. The setup led to a measured suppression factor of 5×10^{-18} for the ^{12}C ion beam. The experiments also indicate that an almost free choice of the charge state for the ^{16}O recoils is possible in the separator.

1 Introduction

The capture reaction $^{12}C(\alpha,\gamma)^{16}O$ ($Q = 7.16$ MeV) takes place during the helium burning stage of Red Giants [1] and is a key reaction of nuclear astrophysics. The cross section at the relevant Gamow-energy, $E_0 \approx 0.3$ MeV, determines not only the nucleosynthesis of elements up to the iron region, but also the subsequent evolution of massive stars, the dynamics of supernovae, and the kind of remnants after supernova explosions. For these reasons, the cross section $\sigma(E_0)$ should be known with a precision of at least 10%. In spite of tremendous experimental efforts over nearly 30 years [2–9], one is still far from this goal. All previous efforts have focused on the observation of the capture γ-rays, including one experiment [5] that combined γ-detection with coincident detection of the ^{16}O recoils produced in the reaction. Due to the low radiative capture cross section and various backgrounds depending on the exact nature of the experiments, γ-ray data with useful, but still inadequate, precision were limited to center-of-mass energies 1.2 MeV $\leq E \leq$ 3.2 MeV, where $E = E_{\rm cm}$ throughout this paper.

To improve the situation, a new experimental approach is in preparation at the 4 MV Dynamitron tandem accelerator in Bochum, called ERNA (**E**uropean **R**ecoil separator for **N**uclear **A**strophysics). In this approach, the reaction is initiated in inverted kinematics, $^4He(^{12}C,\gamma)^{16}O$, i.e. a ^{12}C ion beam is guided into a windowless ^4He jet gas-target and the kinematically forward-directed ^{16}O recoils are detected downstream on the beam line. The direct observation of the ^{16}O recoils requires an efficient recoil separator to filter out the intense ^{12}C beam particles from the ^{16}O recoils: the number of ^{16}O recoils per incident ^{12}C projectile is 1×10^{-18} for $\sigma = 1$ pb and a target density $n(^4He) = 1\times10^{18}$ atoms/cm^2. The recoil separator must also filter out beam contaminants, small-angle elastic scattering products, and background events from multiple scattering processes leading to a degraded tail of the projectiles. If the filtering of the separator is sufficiently effective (with a beam suppression factor of the order $R_{\rm rec} = 1\times10^{-14}$ at $E = 0.7$ MeV), the ^{16}O recoils can be counted directly in a ΔE-E telescope placed in the beam

* Supported in part by the Deutsche Forschungsgemeinschaft (Ro429/35-1) and the Istituto Nazionale di Fisica Nucleare (INFN)
[a] Alexander von Humboldt Fellow
[b] Alexander von Humboldt Award

line at the end of the recoil separator, where the telescope allows for particle identification. Previous measurements [10] have shown that a suppression factor for the telescope alone of $R_{\rm tel} = 1 \times 10^{-4}$ can be achieved leading to a combined suppression factor of $R_{\rm tot} = R_{\rm rec} R_{\rm tel} = 1 \times 10^{-18}$ at $E = 0.7$ MeV for the planned separator.

Since the ^{12}C projectiles and the ^{16}O recoils have essentially the same momentum and since the ^{12}C ion beam emerging from the accelerator passes a momentum filter (analysing magnet), a nearly complete elimination of any ^{16}O beam contaminant in the ^{12}C ion beam incident on the ^{4}He gas target is of utmost importance for the new approach: the ^{16}O beam contaminant and the ^{16}O recoils cannot be distinguished in the recoil separator, since both have the same momentum. In a first ERNA report [11], a Wien filter (WF) and a ΔE-E telescope were used to investigate the ^{16}O beam contamination accompanying a momentum-filtered ^{12}C beam: the intensity ratio of ^{16}O to ^{12}C was found to be about $P_0 = 6 \times 10^{-10}$, i.e. much higher than the intensity ratio 1×10^{-18} between the ^{16}O recoils and the ^{12}C projectiles at $E = 0.7$ MeV, or even 5×10^{-14} at $E = 2.45$ MeV with maximum radiative capture cross section $\sigma \approx 50$ nb.

In recoil separators that include momentum analysis, it is necessary to make a charge state selection of the recoils, causing a reduction in the number of recoils transmitted through the separator. However, since there is usually – in the equilibrium charge state distribution – a charge state representing about 50% of the total recoils produced, this reduction is not too serious. Since the ^{16}O recoils are produced in the ^{4}He jet gas-target, their charge state distribution depends however on the geometric location within the target: those ^{16}O recoils produced in the upstream part of the target will most likely reach an equilibrium charge state distribution in the passage of the remaining target length, while those ^{16}O recoils produced near the downstream end of the target will not. Thus, not all ^{16}O recoils produced will be characterized by an equilibrium charge state distribution and this feature can lead to significant uncertainties in the cross section determination. It was found previously [10], that the charge state distribution of the recoils also depends on the incident charge state of the projectiles, called a memory effect. A possible solution for these problems lies in the installation of an additional gas stripper (e.g. Ar gas) shortly after the jet gas-target, which is presently in the stage of technical development.

Although the ^{16}O recoils – produced in the ^{4}He jet gas-target via the reaction ^{4}He(^{12}C,γ)^{16}O – are kinematically forward-directed, the emission of the capture γ-rays (energy E_γ) leads to an emission cone of half-angle $\theta = \arctan(E_\gamma/pc)$, where p is the momentum of the ^{16}O recoils and c is the velocity of light. Associated with the γ-ray emission there is also a spread $\Delta p/p$ in momentum. For example, at $E = 0.7$ MeV ($E_\gamma = 7.9$ MeV) one finds $\theta = 1.8^\circ$ and $\Delta p/p = 6.2\%$, and at $E = 5.0$ MeV ($E_\gamma = 12.2$ MeV) one finds $\theta = 1.0^\circ$ and $\Delta p/p = 3.6\%$. At $E = 0.7$ MeV, the cone has reached a diameter of 3.1 cm at a 0.5 m distance from the jet gas-target. Thus, shortly after the jet gas-target there must be a focusing element followed by filter elements and other focusing elements up to the site of the telescope, where all elements must have an angle acceptance of at least $\theta = 1.8^\circ$ and a momentum acceptance of at least $\Delta p/p = 6.2\%$, in order to transport the ^{16}O recoils with 100% transmission to the telescope. This requirement demands a compact design of the jet gas-target system involving several pumping stages, where the present technical plan involves an extension of 35 cm on both sides of the jet gas-target.

In summary, the high detection efficiency of the ^{16}O recoils and the negligible contribution of cosmic-ray events in the $\Delta E - E$ coincidences of the telescope probably allow a measurement of the ^{4}He(^{12}C,γ)^{16}O cross section to as low as $E = 0.7$ MeV ($\sigma \approx 1$ pb), if the following requirements can be fulfilled: (i) a ^{12}C beam suppression $R_{\rm rec} = 1 \times 10^{-14}$ in the separator, (ii) a free selection of the charge state for the ^{16}O recoils in the separator, (iii) a relative ^{16}O beam contamination of $P_{\rm tot} \leq 1 \times 10^{-20}$ in the incident ^{12}C beam, (iv) a 100% beam-energy-independent separator detection efficiency of all ^{16}O recoils of the selected charge state emerging from the jet gas-target, and (v) an equilibrium charge state distribution of the ^{16}O recoils after the jet gas-target. In the present work, we report – in Sect. 2 – on calculations of ion beam optics for the filtering and focusing elements of ERNA needed to fulfill the requirement (iv) and – in the subsequent sections – on experimental studies of the requirements (i) to (iii).

2 Ion beam optics

The ^{16}O recoils are produced in the jet gas-target and form nearly a point source. Due to the considerable emittance cone and momentum spread of the ^{16}O recoils ($\theta \leq 1.8^\circ$ and $\Delta p/p \leq 6.2\%$), the recoils need to be focused to a nearly parallel beam at the entrance of the telescope which has a 40 mm-diameter foil window. To fulfill this condition and to have economical and easy tuning of the ^{16}O recoil beam as well as of simulating pilot beams [10], a minimum of focusing elements and apertures of 50 mm maximum diameter should be used. Note that the bulk of the ^{12}C ion beam will be swept out by the first Wien filter after the jet gas-target into a beam stop off the beam line.

The calculations of ion beam optics for the recoil separator ERNA were performed up to third order using the program COSY INFINITY [13]. They showed that the above requirements can be fulfilled with the setup indicated in Fig. 1. After the jet gas-target, the separator will consist sequentially of the following elements: (i) a magnetic quadrupole triplet (QT; length $L = 1050$ mm, inner diameter $\Phi = 106$ mm), (ii) a Wien filter (WF3; Sect. 3), (iii) a magnetic quadrupole singlet (QS1; $L = 52$ mm, $\Phi = 77$ mm), (iii) a Faraday cup (FC3), (iv) a 60° dipole magnet (Sect. 3), (v) a magnetic quadrupole doublet (QD; $L = 508$ mm, $\Phi = 77$ mm), (vi) a Wien filter (WF4; Sect. 3), (vii) a magnetic quadrupole singlet (QS2; $L = 52$ mm, $\Phi = 77$ mm), (viii) a Faraday cup (FC4), and (ix) the $\Delta E - E$ telescope [11].

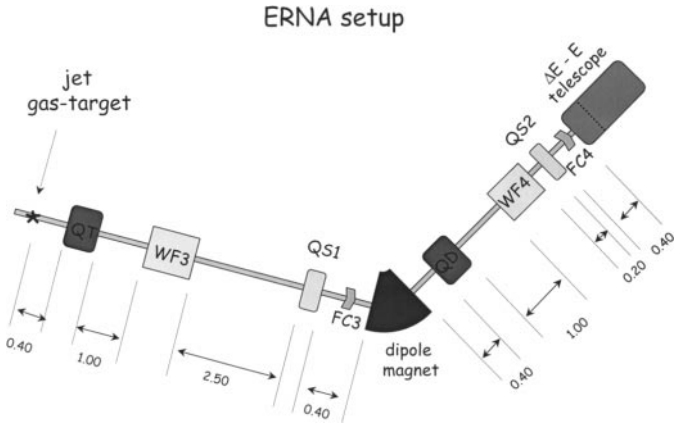

Fig. 1. Schematic diagram of the complete ERNA setup (WF = Wien filter, FC = Faraday cup, QS = quadrupole singlet, QD = quadrupole doublet, QT = quadrupole triplet). The given drift lengths between the components are in units of meters

The calculations were performed assuming a parallel ^{12}C ion beam of 3 mm diameter and a pointlike ^{4}He jet gas-target with a density of 1×10^{18} atoms/cm^2. To calculate the emittance of the ^{16}O recoils, the energy loss of the ^{12}C projectiles and the ^{16}O recoils in the gas target as well as the recoil from the capture γ-rays to the ^{16}O ground state (for assumed isotropic emission) were taken into account; the effects of angle and energy straggling in the target have also been included. The calculations were performed over the planned energy region, $E = 0.7$ to 5.0 MeV, where at each energy the most probable charge state q_0 was selected for the ^{16}O recoils (e.g. $q_0 = 3^+$ for $E = 0.7$ MeV and $q_0 = 6^+$ for $E = 5.0$ MeV).

The optimum drift length between each pair of ERNA elements was calculated with results given in Fig. 1 (e.g. 0.40 m between the jet gas-target and QT). Samples of the resulting $^{16}O^{3+}$ trajectories in the two orthogonal directions perpendicular to the beam axis, are shown in Fig. 2a for $E = 0.7$ MeV, where the following magnetic field strengths have been assumed: $B_{\mathrm{QT}/1} = 0.136$ T, $B_{\mathrm{QT}/2} = 0.150$ T, $B_{\mathrm{WF3}} = 0.080$ T, $B_{\mathrm{QS1}} = 0.058$ T, $B_{\mathrm{QD}/1} = 0.149$ T, $B_{\mathrm{QD}/2} = 0.140$ T, $B_{\mathrm{WF4}} = 0.120$ T, and $B_{\mathrm{QS2}} = 0.025$ T. The resulting $^{16}O^{6+}$ trajectories for $E = 5.0$ MeV are shown in Fig. 2b for the magnetic field strengths $B_{\mathrm{QT}/1} = 0.192$ T, $B_{\mathrm{QT}/2} = 0.211$ T, $B_{\mathrm{WF3}} = 0.110$ T, $B_{\mathrm{QS1}} = 0.074$ T, $B_{\mathrm{QD}/1} = B_{\mathrm{QD}/2} = 0.210$ T, $B_{\mathrm{WF4}} = 0.110$ T, and $B_{\mathrm{QS2}} = 0.025$ T. The trajectories emitted within the entire cone are 100% transmitted to the telescope, where they enter the telescope within a diameter of about 30 mm and are nearly parallel.

3 Equipment and setup

The measurement of the setup specifications was performed with the layout shown in Fig. 3 including a large part of the elements of the ERNA separator.

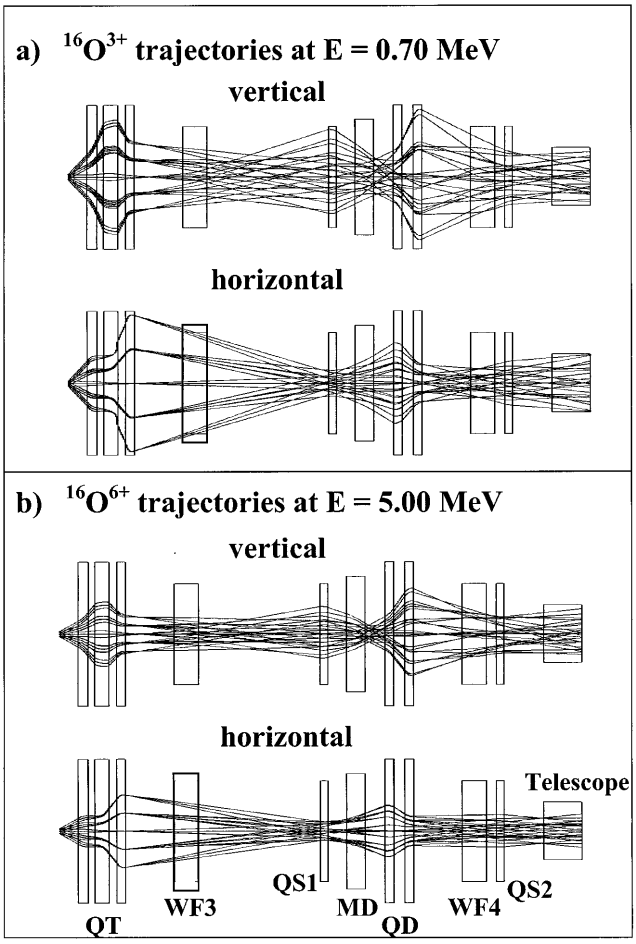

Fig. 2. Samples of ^{16}O trajectories are shown for (**a**) $E = 0.70$ MeV ($q_0 = 3^+$, $\theta_{\max} = 1.9°$, $\Delta E = 0.13$ MeV) and (**b**) $E = 5.0$ MeV ($q_0 = 6^+$, $\theta_{\max} = 1.0°$, $\Delta E = 0.44$ MeV). The trajectories start at the jet gas-target (^{4}He target density $= 1 \times 10^{18}$ atoms/cm^2) and are followed through the filtering and focusing elements of ERNA (indicated by square boxes) up to the telescope (WF = Wien filter, QS = quadrupole singlet, QD = quadrupole doublet, QT = quadrupole triplet, MD = magnetic dipole)

The ^{12}C and ^{16}O ion beams were provided by the 4 MV Dynamitron tandem accelerator at the Ruhr-Universität Bochum. Briefly, a negative ion beam was produced with a sputter ion source at 130 kV potential, then selected by a 90° injection magnet, focused by a gridded lens, and accelerated to the high voltage terminal of the tandem (Fig. 3). After electron stripping within the terminal in nitrogen gas, the positive ions, further accelerated and emerging from the tandem, were focused by a magnetic quadrupole doublet, filtered with respect to momentum and charge state by a 52° analysing magnet, and guided into the 75° beam line by a switching magnet. Finally, a magnetic quadrupole doublet was used to focus the beam for its desired application.

In order to reduce the ^{16}O contamination to a level $P_{\mathrm{tot}} \leq 1 \times 10^{-20}$, we have installed two identical WF [11], WF1 before and WF2 after the analysing magnet

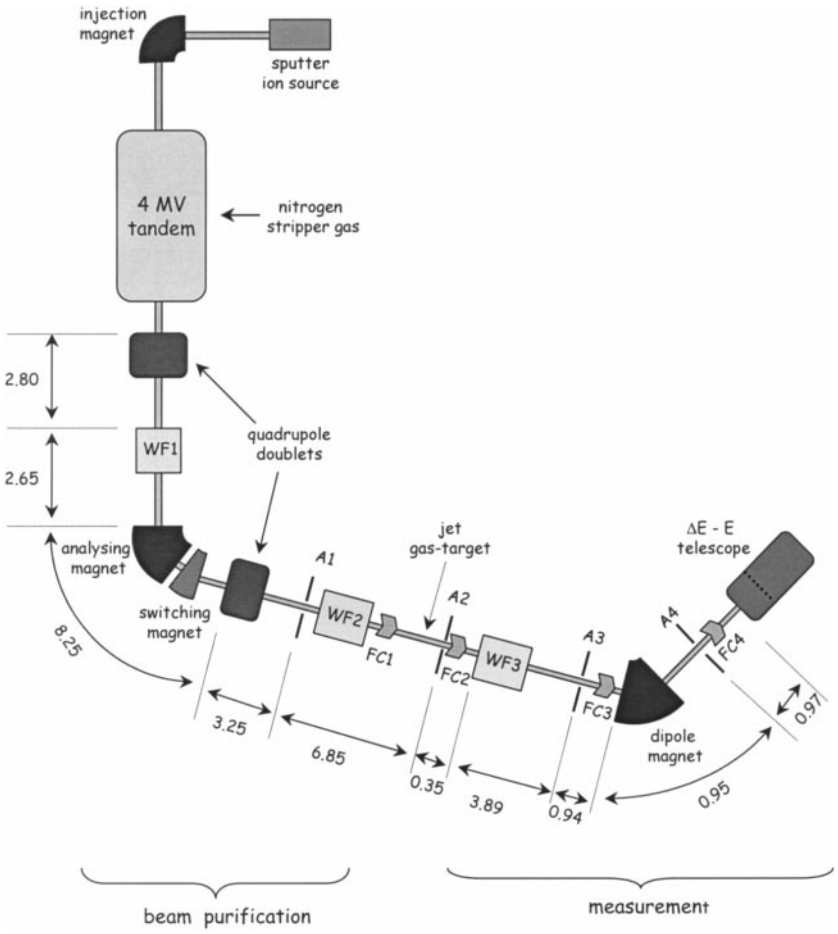

Fig. 3. Schematic diagram of the 4 MV Dynamitron tandem accelerator with relevant components and of the experimental setup (WF = Wien filter, FC = Faraday cup, A = aperture) representing to a large extent the ERNA setup. The given distances are in units of meters

(Fig. 3). The resulting level of ^{16}O purification was measured using (Fig. 3) the combination of a third WF (WF3), a 60° dipole magnet, and a $\Delta E - E$ telescope (ionisation-chamber with an entrance window of 40 mm diameter [11]). For the measurement of the beam suppression factor $R_{\rm rec}$, a fourth WF (WF4) was also involved, which was installed between the dipole magnet and the telescope (not shown in Fig. 3) completing to a large extent the planned ERNA setup (Fig. 1).

The third Wien filter (WF3, *DANFYSIK*) contains two electrostatic plates (120 mm width, 500 mm effective length, 70 mm apart), which are installed on the right and left sides of the beam axis. The electric field is produced by positive and negative voltages applied to the plates (power supplies with analog remote control: *GLASSMAN*, model PS/EL50N; 50 kV/0.8 mA, voltage stability $< 1 \times 10^{-4}$ over 8 hours). The Wien filter also involves two separate pole faces (320 mm width, 500 mm effective length, 160 mm apart) installed above and below the beam pipe. The lateral uniformity of the magnetic field is 0.1% over a distance of 16 mm on both sides of the beam axis; along the beam axis, the magnetic field is homogeneous within 1% and drops sharply near the edges of the pole faces. The power supply for the magnetic field (*DANFYSIK*, model 858; 120A/42V) has a current stability of 1×10^{-5} over 8 hours.

The fourth Wien filter (WF4, from Caltech) contains two electrostatic plates (63 mm width, 578 mm effective length, 70 mm apart), which are installed on the right and left sides of the beam axis and driven by a power supply identical to that for WF3. The two pole faces (77 mm width, 578 mm effective length, 95 mm apart) are installed above and below the beam pipe. The lateral magnetic field uniformity is 0.1% over a distance of 25 mm on both sides of the beam axis; along the beam axis, the magnetic field is homogeneous within 1% and drops sharply near the edges of the pole faces. The power supply for the magnetic field (FUG, model MCN1400/650; 2A/650V) has a current stability of better than 1×10^{-5} over 8 hours.

The 60° dipole magnet (also from Caltech) of 400 mm radius of curvature and 76 mm gap spacing is driven by a power supply with analog remote control (*DANFYSIK*, model 853; 150A/150V, current stability (1×10^{-6} over 8 hours).

The magnetic fields of all relevant elements were measured using commercial or home-made tesla meters [11].

4 Experimental procedures and results

With all Wien filters switched off, the momentum-filtered ^{12}C beam was first focused through aperture A1 ($\Phi = 40$

mm) on Faraday cup FC1 (Fig. 3), then through A2 ($\Phi =$ 8 mm) on FC2 and through A3 ($\Phi = 8$ mm) on FC3, and finally through A4 ($\Phi = 7$ mm) on FC4, where in the last step the magnetic field of the 60° dipole magnet was set appropriately. Note that both the ^{12}C ion beam and its ^{16}O beam contamination – having the same charge and momentum – will arrive at FC4. Variation of the incident ^{12}C energy (momentum) and observation of the resulting current on FC4 led to a momentum acceptance $\Delta p/p =$ 1.1% for the dipole magnet, for the given apertures.

Each Wien filter was then turned on separately, and for the chosen value of the electric field (i.e. the voltages $+U$ and U applied to the plates: $U_{\max} = 20$, 20, and 40 kV for WF1, WF2, and WF3, respectively), the corresponding value of the magnetic field B was determined for optimum beam transmission, which did not change significantly ($\leq 10\%$). The observed velocity acceptances are $\Delta v/v = 1.6$, 0.6, and 3.0% for WF1, WF2, and WF3, respectively.

The projectile suppression factor R is defined as the ratio of the number of beam particles N_t transmitted through both WF3 and the 60° dipole magnet, when both are on, to the number of incident particles N_i, i.e. with WF3 off. In these measurements, WF1 and WF2 were both off. The incident flux N_i was determined by the beam current at FC4 preceding the telescope. With the voltage producing the electric field set at $U_{\mathrm{WF3}} = 40$ kV, the transmitted flux N_t after WF3 was determined as a function of the magnetic field strength B_{WF3}, either via current measurement at FC4 (for high N_t values) or with the telescope (for low N_t values). The resulting suppression factor for a $^{12}C^{3+}$ ion beam with $E_{\mathrm{lab}} = 10$ MeV is shown in Fig. 4, where the nearly flat part with $R_{\mathrm{rec}} = 1 \times 10^{-10}$ represents the degraded tail of the projectiles. The ^{12}C peak at $B(^{12}\mathrm{C}) = 137$ mT has a FWHM $\Delta B = 3.2$ mT ($\Delta B/B = 2.4\%$).

A field strength $B(^{16}\mathrm{O}) = 4/3B(^{12}\mathrm{C}) = 182$ mT corresponds to the velocity of a contaminant ^{16}O beam which could – in the planned ^{4}He(^{12}C,()^{16}O experiment – correspond to the velocity of the ^{16}O recoils. The $\Delta E - E$ identification matrix of the telescope [11] (Fig. 5a) obtained at this field strength verifies the presence of a contaminant ^{16}O beam, whose peak intensity drops at other field strengths (Fig. 4) with a FWHM $\Delta B = 3.2$ mT ($\Delta B/B = 1.8\%$), similarly to that of the ^{12}C projectiles. The energy of the contaminant ^{16}O beam is about $\frac{3}{4}$ the energy of the ^{12}C incident beam, as expected from the momentum filter for equal charge states, and corresponds to a section of a degraded ^{16}O tail produced in the tandem accelerator. The intensity ratio of the ^{16}O peak to the ^{12}C peak (Fig. 4) is $P_0 = 1 \times 10^{-11}$, a value similar to that reported previously. It was found [11], that the main source of the ^{16}O beam contamination lies in the ion source setup, arising from the presence of oxygen in the sputter material and the finite mass resolution of the injection magnet. In order to minimize the intensity of the contaminant ^{16}O beam, we used nitrogen (rather than the usual oxygen) as the stripper gas in the terminal of the tandem.

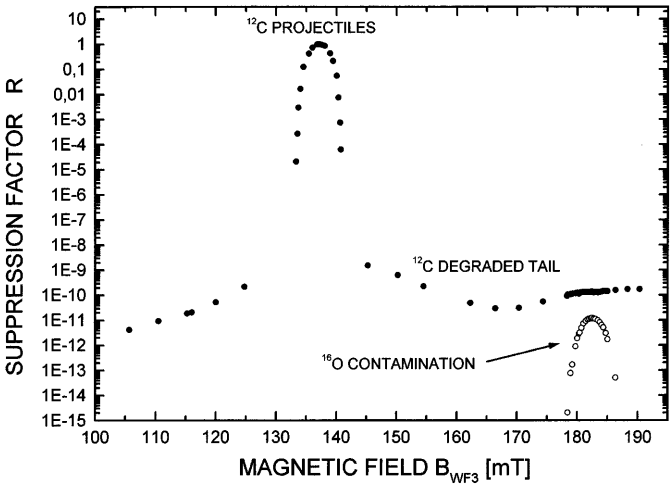

Fig. 4. Suppression factor R of a 10 MeV momentum-filtered $^{12}C^{3+}$ ion beam achieved with the Wien filter WF3 and the 60° dipole magnet. The ^{12}C peak at $B_{\mathrm{WF3}} = 137$ mT has a FWHM of 3.2 mT. Another peak – observed at 182 mT (FWHM = 3.2 mT) with the telescope – is identified as a contaminant ^{16}O beam in the incident beam from the accelerator, with the same momentum and charge state as the incident ^{12}C ion beam

As a next step, the beam-purifying WF1 (Fig. 3) was set at the velocity $v(^{12}\mathrm{C})$ to transmit the ^{12}C ion beam. After 2 hours of running, the $\Delta E - E$ identification matrix of the telescope showed no ^{16}O events leading to a purification factor for WF1 of $P_{\mathrm{WF1}} < 1 \times 10^{-7}$ with regard to the number of ^{16}O counts in Fig. 5a. In order to measure the actual value of P_{WF1}, the ^{16}O flux had to be increased. For this reason, an $^{16}O^{3+}$ ion beam of $E_{\mathrm{lab}} = 7.50$ MeV (i.e. with the same momentum as the 10.0 MeV $^{12}C^{3+}$ ion beam) was produced leading to a 5.9 μA current at FC4, with WF1 off. The WF1 was then set at $v(^{12}\mathrm{C})$ and the identification matrix showed an $^{16}O^{3+}$ peak (Fig. 5b), whose count rate relative to the 5.9 μA $^{16}O^{3+}$ current led to $P_{\mathrm{WF1}} = 1.0 \times 10^{-12}$ (Fig. 6a) The same procedure was repeated for the other beam-purifying WF2 (but with WF1 off) with the result $P_{\mathrm{WF2}} = 1.4 \times 10^{-12}$ (Fig. 6b). If one assumes the validity of a multiplication of the purification levels for WF1 and WF2, one arrives at $P_{\mathrm{WF1+WF2}} = P_{\mathrm{WF1}} P_{\mathrm{WF2}} = 1.4 \times 10^{-24}$. A direct measurement showed no events after 14 hours of running and led experimentally to $P_{\mathrm{WF1+WF2}} < 2 \times 10^{-18}$. We arrive therefore at a residual ^{16}O contamination of $P_{\mathrm{tot}} = P_{\mathrm{WF1+WF2}} P_0 < 2 \times 10^{-29}$ (and most likely $P_{\mathrm{tot}} = 1.4 \times 10^{-35}$) for the ERNA project setup.

The identification matrix (Fig. 5a) shows events along the expected location for ^{12}C ions, which arise from the degraded tail of the incident ^{12}C ion beam (e.g. due to multiple scattering on the apertures). The number of counts of all ^{12}C events leads to the suppression factor $R_{\mathrm{rec}} = 1 \times 10^{-10}$ quoted above. A closer inspection of Fig. 5a reveals two ^{12}C peaks corresponding to the velocity- and momentum-filtered sections of the degraded tail of the ^{12}C beam: the peak to the left has $E_{\mathrm{lab}} \approx 5$

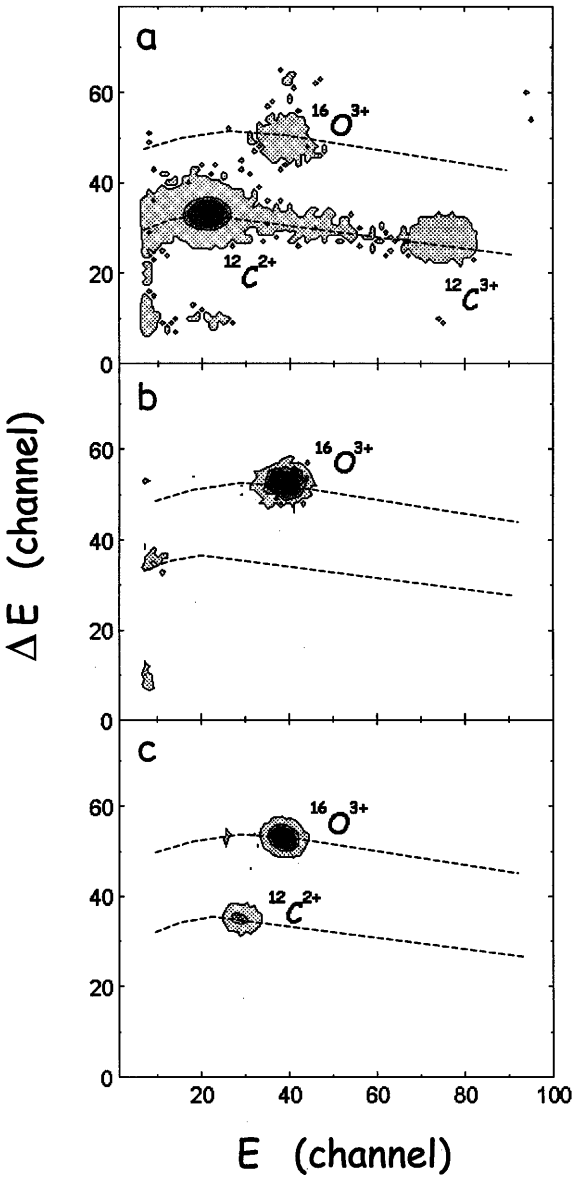

Fig. 5. The $\Delta E-E$ identification matrix for a $^{12}C^{3+}$ ion beam of 10 MeV is shown with (**a**) WF3 tuned to $v(^{16}O) = \frac{3}{4}v(^{12}C)$ and (**b**) WF2 tuned to $v(^{12}C)$ and WF3 tuned to $v(^{16}O)$. In the case (**a**), the injection magnet of the ion source was set at mass 12, and in the case (**b**) it was set at mass 16: the contaminant ^{16}O beam appears at the same point in the matrix. Another identification matrix for the above ^{12}C ion beam is shown in (**c**) with WF1 and WF2 off while WF3, the dipole magnet, and WF4 were tuned to $v(^{16}O)$. The dashed curves correspond to the expected locations of ^{12}C and ^{16}O ions in the matrix

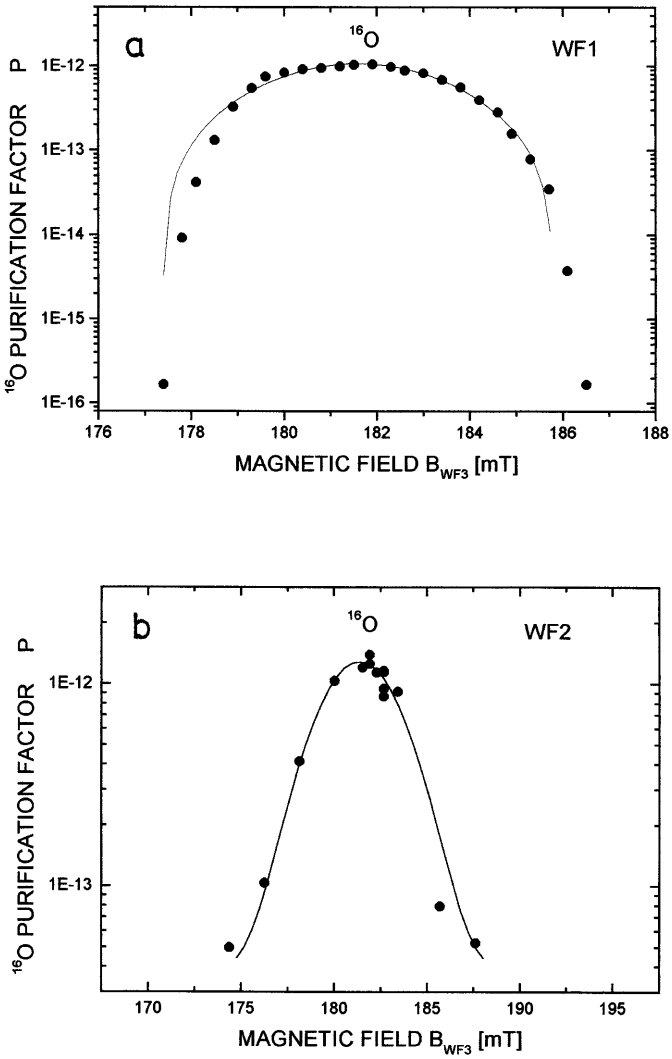

Fig. 6. The ^{16}O purification factor is shown as a function of magnetic field strength B_{WF3} for (**a**) WF1 alone and (**b**) WF2 alone. The solid curves are fits assuming Gaussian functions

MeV and charge state $q_C = 2^+$ and that to the right has $E_{lab} \approx 10$ MeV and $q_C = 3^+$. Since ERNA will involve an additional WF (WF4) after the 60° dipole magnet, its filtering action will only pass a small section near the 2^+ ^{12}C peak. To measure the beam suppression factor for this final ERNA layout, we installed WF4 (Fig. 1 and Sect. 3) and an additional Faraday cup after WF4. The resulting identification matrix (Fig. 5c) leads to a beam suppression factor of $R_{rec} = 1\times10^{-13}$. The count rate was 0.25/s, while the telescope can handle a count rate of about 5 kHz, thus $R_{tel} = 5 \times 10^{-5}$ and $R_{tot} = R_{rec}R_{tel} = 5 \times 10^{-18}$, a value close to the ERNA requirement.

5 Discussion

The ^{16}O beam contamination relative to the incident momentum-filtered ^{12}C ion beam (with $E_{lab} = 10$ MeV) could be reduced from $P_0 = 1 \times 10^{-11}$ to $P_{tot} < 2 \times 10^{-29}$ (and most likely to $P_{tot} = 1.4 \times 10^{-35}$) by the installation of Wien filters both before and after the analysing magnet. It should be pointed out that the purification level of each Wien filter as well as that of their combination could be measured only with an intense ^{16}O beam

of $E_{\rm lab} = 7.5$ MeV, where the beam optics up to Faraday cup FC4 (Fig. 3) was nearly identical to that of the ^{12}C beam ($E_{\rm lab} = 10$ MeV) with the same momentum. Since the ^{16}O beam contamination represents a section of a degraded ^{16}O tail, it may have a somewhat different purification level than an ^{16}O beam. However, assuming an uncertainty of several orders of magnitude, the purification level is still far better than the level required by ERNA ($P_{\rm tot} \leq 10^{-20}$).

The setup used for the measurement of the beam suppression factor is nearly identical to that in the final ERNA layout, where a compact jet gas-target system will be installed between WF2 and WF3 (Fig. 3). Between WF3 and the dipole magnet there will be a sizable side port used as a ^{12}C beam dump, whereby the intense ^{12}C beam – deflected by WF3 – will be removed effectively from the beam axis. We have simulated this side port in the present studies by the installation of a 30 cm-long pipe ($\Phi = 17$ mm, otherwise completely closing the beam pipe) in the $4''$ beam pipe at a 1.5 m distance downstream from WF3, where the deflected ^{12}C beam was hitting the $4''$ beam pipe at a point downstream of the entrance of the 30 cm-long pipe.

The experiments indicate that a free choice of the charge state for the ^{16}O recoils is possible (here: $q_{\rm C} = q_O = 3^+$). The exception is the charge state combination $q_{\rm C} = 3^+$ and $q_O = 4^+$, for which the momenta and velocities of ^{12}C and ^{16}O are identical (due to their mass ratio $\frac{3}{4}$) and thus no filtering is possible with ERNA. However, this represents no serious problem: at high energies (say $E_{\rm lab} \geq 5$ MeV) one may choose $q_{\rm C} = 3^+$ and $q_0 = 5^+$ (or 6^+) or $q_{\rm C} = 4^+$ and $q_0 = 5^+$ (or 6^+), while at low energies one can choose $q_{\rm C} = 2^+$ and $q_0 = 3^+$ (or 4^+). In all these cases, the charge state probability for the ^{16}O recoils is of the order of 50%: e.g. at $E_{\rm lab}(q_{\rm C} = 4^+) = 20$ MeV one finds [12] a probability $\varphi(q_0 = 6^+) = 49\%$, and at $E_{\rm lab}(q_{\rm C} = 2^+) = 4.0$ MeV one finds $\varphi(q_0 = 4^+) = 45\%$.

References

1. C. Rolfs and W.S. Rodney: Cauldrons in the Cosmos (University of Chicago Press, 1988)
2. P. Dyer, C.A. Barnes: Nucl. Phys. A**233** (1974) 495
3. K.U. Kettner, H.W. Becker, L. Buchmann, J. Görres, H. Kräwinkel, C. Rolfs, P. Schmalbrock, H.P. Trautvetter, A. Vlieks: Z. Phys. A**308** (1982) 73
4. A. Redder, H.W. Becker, C. Rolfs, H.P. Trautvetter, T.R. Donoghue, T.C. Rinkel, J.W. Hammer, K. Langanke: Nucl. Phys. A**462** (1987) 385
5. R.M. Kremer, C.A. Barnes, K.H. Chang, H.C. Evans, B.W. Filippone, K.H. Hahn, L.W. Mitchell: Phys. Rev. Lett. **60** (1988) 1475
6. J.M.L. Ouellet, H.C. Evans, H.W. Lee, J.R. Leslie, J.D. MacArthur, W. McLatchie, H.B. Mak, P. Skensved, J.L. Witton, X. Zahao, T.K. Alexander: Phys. Rev. C**54** (1996) 1982
7. G. Roters, C. Rolfs, F. Strieder, H.P. Trautvetter: Eur. Phys. J. (in press)
8. D. Rogalla, Diplomarbeit, Ruhr-Universität Bochum (1997); D. Rogalla, L. Gialanella, U. Greife, C. Rolfs, F. Schümann, F. Strieder, H.P. Trautvetter: Eur. Phys. J. (to be submitted)
9. L. Gialanella, Thesis, Ruhr-Universität Bochum (1999), to be published
10. L. Gialanella, F. Strieder, K. Brand, L. Campajola, A. D'Onofrio, U. Greife, E. Huttel, F. Petrazzuolo, V. Roca, C. Rolfs, M. Romano, M. Romoli, S. Schmidt, W.H. Schulte, F. Terrasi, H.P. Trautvetter, D. Zahnow: Nucl. Instr. Meth. A**376** (1996) 174
11. D. Rogalla, S. Theis, L. Campajola, A. D'Onofrio, L. Gialanella, U. Greife, G. Imbriani, A. Ordine, V. Roca, C. Rolfs, M. Romano, C. Sabbarese, F. Schümann, F. Strieder, F. Terrasi, H.P. Trautvetter: Nucl. Instr. Meth. (in press)
12. J.B. Marion, F.C. Young: Nuclear Reaction Analyses (Elsevier, 1968)
13. M. Berz: Computational aspects of design and simulation (COSY INFINITY), Nucl. Instr. Meth. A**298** (1990) 473